Low-Cost PEM Fuel Cell Diagnosis Based on Power Converter Ripple With Hysteresis Control

Giovanni Dotelli, Roberto Ferrero, *Member, IEEE*, Paola Gallo Stampino,
Saverio Latorrata, and Sergio Toscani, *Member, IEEE*

NOMENCLATURE

T_{sw}, f_{sw}	Converter switching period and frequency.
δ	Converter duty cycle.
T_{ON}, T_{OFF}	Closed and open switch times.
ΔI	Current ripple peak-to-peak amplitude.
i_m, v_m	Low-frequency FC current and voltage.
i_{hf}, v_{hf}	High-frequency current and voltage ripple.
I_{hf}, V_{hf}	High-frequency current and voltage spectra.
Z_{hf}	High-frequency FC impedance.
L_b, C_b	Converter inductance and capacitance.
R_{trans}, C_{trans}	FC transport resistance and capacitance.
R_{act}, C_{act}	FC activation resistance and capacitance.
R_{ohm}	FC ohmic resistance.
L_s	FC and connections inductance.
t_k, i_k, v_k	Time, current and voltage sequences.
T_s	Sampling period.
N	Number of samples involved in the fitting.
$\sigma^2(\cdot)$, $\sigma(\cdot,\cdot)$	Variance and covariance.
$u(\cdot)$	Standard uncertainty.
$(\cdot)_{est}$, $\overline{(\cdot)}$	Estimated values and their averages.
$(\cdot)_{ON}$, $(\cdot)_{OFF}$	Values referred to T_{ON} and T_{OFF}.
$(\cdot)_r$	Values in one current or voltage ramp.

Manuscript received January 28, 2015; revised April 16, 2015; accepted April 28, 2015. Date of publication June 1, 2015; date of current version October 7, 2015. The Associate Editor coordinating the review process was Dr. Serge Demidenko.

G. Dotelli, P. G. Stampino, and S. Latorrata are with the Department of Chemistry, Materials, and Chemical Engineering G. Natta, Politecnico di Milano, Milan 20133, Italy (e-mail: giovanni.dotelli@polimi.it; paola.gallo@polimi.it; saverio.latorrata@polimi.it).

R. Ferrero is with the Department of Electrical Engineering and Electronics, University of Liverpool, Liverpool L69 3GJ, U.K. (e-mail: roberto.ferrero@liverpool.ac.uk).

S. Toscani is with the Dipartimento di Elettronica, Informazione e Bioingegneria, Politecnico di Milano, Milan 20133, Italy (e-mail: sergio.toscani@polimi.it).

Color versions of one or more of the figures in this paper are available online.

I. INTRODUCTION

THE increasing emergence on the market of commercial devices powered by fuel cells (FCs) urgently demands the development of low-cost diagnostic tools to guarantee reliable long-term operation at an affordable price suitable for massive-scale market diffusion of these devices. In particular, for polymer electrolyte membrane (PEM) FCs, which represent one of the most promising technologies for mobile and powertrain applications [1], [2], an effective water management is one of the main goals that needs to be achieved, as the cell water content deeply affects the cell efficiency, voltage stability, and lifetime [3], [4].

It is well known that a wealth of information about the FC state of health can be obtained by electrochemical impedance spectroscopy (EIS). Indeed, impedance measurements at different frequencies provide insight into the different electrochemical phenomena that characterize the complex FC behavior, thus allowing to well distinguish between different causes of performance degradation [5]. As far as water management is concerned, the two opposite failure modes, namely, membrane dehydration and cell flooding, produce a significant increase in the equivalent ohmic and transport resistances, respectively. Since the former represents the main contribution to the high-frequency FC impedance (above 1 kHz) while the latter represents the main contribution to the low-frequency impedance (below 1 Hz), EIS is commonly employed in laboratory experiments to detect membrane dehydration and cell flooding [6]–[9].

It is also known, however, that the complex and expensive instrumentation used in laboratories for conventional EIS (typically involving a frequency response analyzer) is not affordable in commercial applications, and thus low-cost solutions for impedance monitoring need to be developed. With this aim, the use of switch-mode power converter ripple for high-frequency impedance measurements was suggested in

a few papers in the literature as a cost-effective approach to estimate the FC ohmic resistance [10], [11]. Previous works of the authors showed how a model-based elaboration of the FC response to the converter ripple in the frequency domain can provide accurate ohmic resistance estimates suitable for diagnostic purposes [12] and the proposed approach was successfully tested with a specifically designed dc/dc converter [13]. References [14] and [15] also showed how *ad hoc* injection of lower-frequency components in the ripple waveform allows one to measure the lower-frequency impedance as well as the ohmic resistance.

All these papers referred to converter operation with constant switching frequency, as in the case of pulsewidth modulation (PWM) control, which is the simplest condition from the impedance measurement point of view because the FC is excited at constant frequencies (the switching frequency and higher harmonics around its multiples) and the signal acquisition can be synchronized with the switching signal, thus avoiding spectral leakage errors. On the other hand, converter control techniques involving variable switching frequencies make the impedance estimation more troublesome, because of the nonsteady-state condition of the FC during measurements and the lack of synchronization between sampling and excitation signals.

This paper discusses these issues focusing on the case study of a dc/dc converter operated with hysteresis control, which represents the simplest solution from the implementation point of view, and it is therefore particularly suitable for low-cost commercial applications. In more details, this paper is organized as follows. After a brief introduction on the hysteresis control of dc/dc converters (Section II) and on FC equivalent circuits (Section III), the classic frequency-domain analysis for ohmic resistance identification, based on the Fourier transform, is compared with a time-domain analysis with a simple model-based identification algorithm, which is shown to be the most convenient solution for accurate real-time ohmic resistance measurements (Section IV). The proposed approach is finally tested on a single PEM FC connected to a low-voltage dc/dc converter, and the elaboration algorithm is implemented in a field-programmable gate array (FPGA) interfaced with a real-time processor (Sections V and VI).

II. DC/DC Converter With Hysteresis Control

The range of FC applications is extremely wide, and they are usually classified into three broad areas: 1) stationary power generation [16]; 2) mobile power generation [17]; and 3) powertrain applications [18]. In most of them, the FC is not directly connected to the load to be fed, but proper power converters are interposed; basically, the reasons are two. The first one is the need to decouple the voltage of the FC stack from that applied to the load; sometimes the load requires an ac voltage [19], or in other cases, it has to be supplied with a dc voltage that is different from that ensuring optimal operation of the stack. However, even when the voltage required to feed the load is similar to the rated voltage of the stack, a dc/dc converter is often needed since

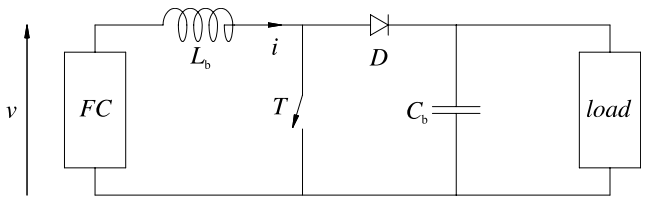

Fig. 1. Schematic of a dc/dc boost converter connected to the FC on one side and to an electrical load on the other side.

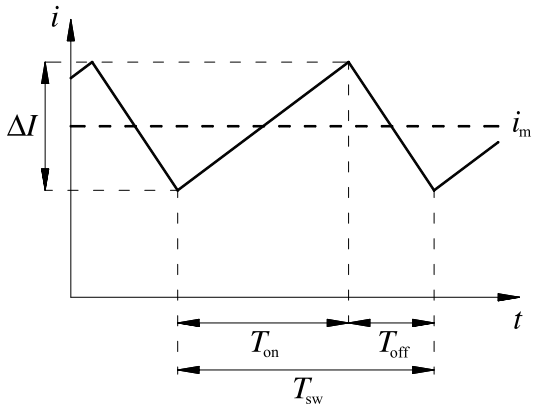

Fig. 2. Theoretical current waveform produced by the dc/dc converter.

the output voltage of a FC is heavily affected by the current, because of the nonnegligible output resistance. The other reason is that a FC has a fairly slow dynamics, so that it is not able to quickly change its power output. Therefore, when the power of the load to be supplied is characterized by large and abrupt variations, the FC has to be integrated with other energy sources, thus forming an hybrid FC system [20], [21]. Power converters and their controls are of utmost importance in this case, since they permit to optimize the exploitation of the sources. In particular, the FC stack may operate in quasi-steady-state conditions, with great advantages in terms of efficiency and power output.

Because of the multifold applications of FC technology, the architectures of the power electronic converters are extremely variegated. However, in many of them, it is necessary to boost the stack voltage, which is not high enough for the application. For this reason, the stack is often connected to a step-up dc/dc converter that boosts the voltage, while ensuring a nearly constant current operation. Although many high-efficiency soft-switching converters have been proposed, the architecture shown in Fig. 1 is still widely employed thanks to its simplicity. As introduced before, the boost chopper is operated to control the cell current. Because of the switching, the current contains a triangular ripple superimposed to the low-frequency component i_m, as shown in Fig. 2, where ΔI is the peak-to-peak amplitude of the ripple and $T_{\rm sw}$ is the switching period, while $T_{\rm ON}$ and $T_{\rm OFF}$ are the durations of the time intervals when the switch T is closed and open, respectively. The relation between ripple amplitude and switching frequency can be written as:

$$\Delta I = \frac{v_m}{f_{\rm sw} L_b}\delta \tag{1}$$

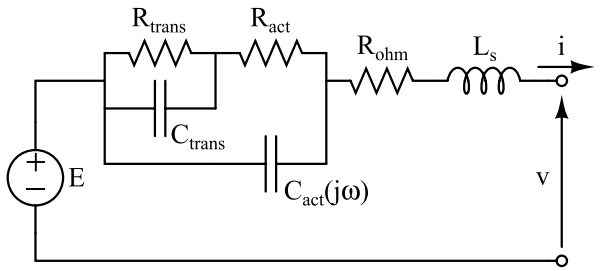

Fig. 3. Typical linearized equivalent circuit of a PEM FC.

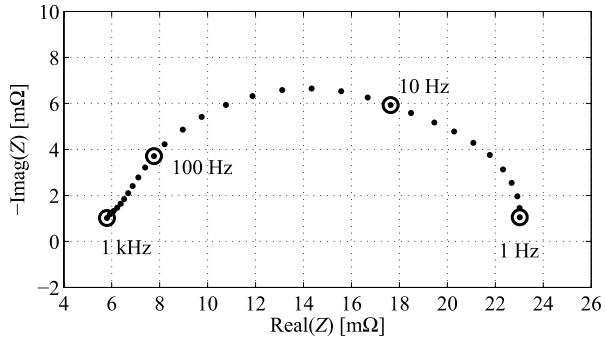

Fig. 4. Impedance spectrum of the cell under test, measured at 9.2-A dc current in typical operating conditions.

where $f_{\rm sw}$ is the switching frequency, L_b the inductance of the boost converter input inductor, δ the duty cycle of the converter, and v_m the low-frequency component of the FC voltage.

PWM and hysteresis modulation are the most common techniques to control the current; the first one operates at constant switching frequency, while the ripple amplitude depends on the working conditions. On the other hand, when hysteresis control is employed, the ripple amplitude ΔI is kept constant, and therefore, according to (1), the switching frequency depends on the operating conditions. Its dynamic performances are good and the implementation is extremely simple: just a current transducer and a Schmitt trigger are required. Even in this case, the current ripple can be exploited to estimate the high-frequency resistance of the FC; however, the measurement becomes much more challenging with respect to a PWM chopper because of the variable switching frequency.

III. Fuel Cell Equivalent Circuit

The equivalent circuit shown in Fig. 3 is often employed as a linearized model to describe the behavior of a PEM FC when it operates around a stable working point. The three equivalent resistances take into account the three main sources of losses, namely, ohmic losses ($R_{\rm ohm}$), activation polarization ($R_{\rm act}$), and mass transport limitation ($R_{\rm trans}$), while the two equivalent capacitances describe the dynamic response associated with activation ($C_{\rm act}$) and transport ($C_{\rm trans}$) phenomena. Frequency dependence of the activation capacitance or a constant-phase element instead of it are usually introduced for a better approximation of the actual cell dynamics [8], [22]. Finally, a series inductance (L_s) may be necessary to take into account inductive phenomena mainly associated with the electrical connections that may appear at high frequencies.

It should be noted that a great variety of equivalent circuits for PEM FCs can be found in the literature (see [1], [23], and [24]). However, they mainly differ in the low-frequency part, associated with the activation and transport processes, which may vary from cell to cell depending on the cell design, while it is generally agreed that the high-frequency limit of the equivalent circuit can be represented by a resistance, with the possible addition of a series inductance to include the inductive effects of electrical connections.

The cutoff frequencies of the two RC circuits (or other equivalent circuits in different models) associated with activation polarization and mass transport limitations are far below typical dc/dc converter switching frequencies (about 10 kHz or even higher), as confirmed by the impedance spectrum of the cell under test shown in Fig. 4, which was measured at medium dc current in typical operating conditions (Sections V and VI). This means that the FC response to the current ripple produced by the converter does not contain any significant capacitive contribution, while it may show an inductive behavior depending on the converter switching frequency and the electrical connections. Therefore, a deeper discussion of low-frequency equivalent circuits falls out of the purposes of this paper, and a first-order RL model is generally expected to be sufficiently accurate to describe the high-frequency response

$$Z_{\rm hf}(j\omega) = -\frac{V_{\rm hf}(j\omega)}{I_{\rm hf}(j\omega)} = R_{\rm ohm} + j\omega L_s \tag{2}$$

which can be also written in the time domain as

$$v_{\rm hf}(t) = -R_{\rm ohm} i_{\rm hf}(t) - L_s \frac{di_{\rm hf}(t)}{dt}. \tag{3}$$

It is now apparent that the high-frequency current ripple inherently produced by the converter allows one to estimate the ohmic resistance value, which is strongly dependent on the membrane water content, and it is therefore a good indicator for membrane dehydration diagnosis. Furthermore, the addition of lower-frequency components in the ripple waveform allows one to estimate other relevant parameters of the FC equivalent circuit, such as the transport resistance, which is a reliable index for detecting cell flooding or gas starvation. Because of the large separation between the converter switching frequency and the frequencies required to identify the low-frequency equivalent circuit parameters, the measurement issues arising from the time-varying switching frequency mentioned in the previous section do not affect the low-frequency measurements. Thus, in the following sections, only the identification of the ohmic resistance from the inherent converter ripple will be discussed.

IV. Ohmic Resistance Identification Algorithms

Several methods for FC ohmic resistance measurements are known in the literature (see [25]). EIS is certainly the most common technique employed in laboratory experiments, while among the methods not requiring expensive dedicated

instrumentation, the most common one is the current interruption technique, which identifies the ohmic resistance from the voltage step following a current step from the load current to zero. The main drawback of this method is the significant perturbation imposed to the system that makes it not suitable for frequent repetition, without mentioning the possible difficulties related to the correct identification of the ohmic voltage step.

The use of the converter ripple represents therefore an interesting alternative for low-cost measurements. Simplified elaboration algorithms were proposed in [10] and [11], but more accurate results require carefully taking into account the nonsinusoidal nature of the ripple and the nonresistive response of the cell, either in the frequency or in the time domain.

A. Frequency-Domain Analysis

To reduce the computational burden, the Fourier transform for the calculation of voltage and current spectra is typically applied to signals acquired in a fixed time window, corresponding to the theoretical period of the signals or an integer multiple of it. In PWM converters, the switching period is known because it is externally imposed, but when hysteresis control is employed, the switching period may significantly differ from the theoretical value and it is also subject to continuous and unpredictable variations. This means that if the Fourier transform is applied on a time window equal to the theoretical switching period, significant leakage errors are likely to appear in the voltage and current spectra, preventing from obtaining meaningful impedance measurements even if the voltage and current spectra are averaged over a much longer time window.

As a possible solution to decrease the effects of leakage errors, a time window equal to several (nominal) switching periods could be considered for the application of the Fourier transform. In this case, any systematic difference between the actual and theoretical switching periods would produce negligible leakage effects. However, the position of the most significant harmonic component in the voltage and current spectra is *a priori* unknown, and therefore, it should be empirically found to obtain meaningful results. Furthermore, if the switching frequency is changing within the observation window, the signal energy is distributed among several harmonic components, so that if a single component is considered, the impedance measurement may be affected by a poor signal-to-noise ratio. A weighted average of the impedance obtained from different spectral components would then be necessary to obtain accurate results.

In conclusion, this last method is the only solution able to provide accurate impedance measurements. However, it is quite complex from the computational point of view, because it requires applying the Fourier transform to voltage and current signals involving a large number of samples and calculating several harmonic components and the corresponding impedance values, to finally average these values with proper weighting coefficients. It is therefore apparent that this solution is not convenient for real-time implementation in commercial applications requiring low-cost instrumentation.

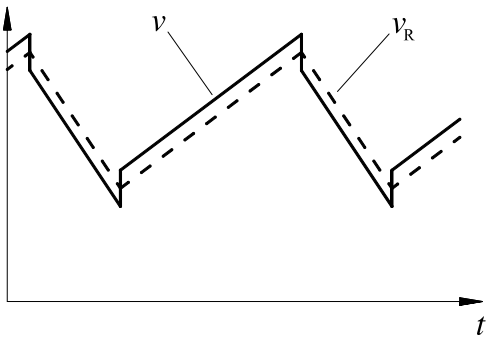

Fig. 5. Voltage response to the converter current ripple (solid line) according to the RL model (3) and its resistive component (dashed line).

As a final remark, it is worth mentioning that the voltage and current ripple signals may be affected by significant disturbances at the time instants corresponding to the converter switching, and such disturbances could represent another important uncertainty source in frequency-domain impedance measurements. To overcome all these issues, a time-domain approach is proposed in Section IV-B as a possible solution.

B. Time-Domain Analysis

The triangular current ripple waveform produced by the converter and the simple FC model (3) describing the cell response to the converter ripple suggest the possibility to estimate the ohmic resistance by a time-domain analysis. Since the FC output impedance at the ripple frequencies is much lower than the impedance of the boost inductor, the power converter behaves, essentially, like a current generator. Therefore, it injects a current waveform that is composed of alternate increasing and decreasing ramps (Fig. 2), and each ramp gives rise to a corresponding voltage ramp according to (3). The opposite of the ratio between the voltage and current slopes is equal to the ohmic resistance R_{ohm}, while the series inductance L_s, if present, produces only an offset in the voltage ramp that does not affect its slope. This is shown in Fig. 5.

Therefore, if each ramp of the voltage and current waveforms is fitted by a straight line, two estimates of the ohmic resistance can be obtained in each switching period. The advantage of this approach is that it does not require the switching period to be constant. It only requires acquiring the digital switching signal to know when each ramp starts and ends. Moreover, the extreme points of each ramp can be excluded from the fitting procedure so that any disturbances introduced on the signals by the commutations, such as fast spikes, do not affect the ohmic resistance estimate, which is contrary to what happens with the Fourier analysis described above.

It is worth noting that the proposed identification algorithm is quite simple and it is therefore suitable for real-time implementation. Indeed, assuming that the differences between

the measured signal and the ideal ramp are only due to random white noise, the classic linear regression algorithm based on the least-squares method provides the following expressions for the slope estimates of the voltage and current ramps:

$$\left.\frac{dv}{dt}\right|_{\text{est}} = \frac{\sigma(t,v)}{\sigma^2(t)} = \frac{N\sum_k t_k v_k - \sum_k t_k \sum_k v_k}{N\sum_k t_k^2 - \left(\sum_k t_k\right)^2} \tag{4}$$

$$\left.\frac{di}{dt}\right|_{\text{est}} = \frac{\sigma(t,i)}{\sigma^2(t)} = \frac{N\sum_k t_k i_k - \sum_k t_k \sum_k i_k}{N\sum_k t_k^2 - \left(\sum_k t_k\right)^2} \tag{5}$$

where $k = 1, \ldots, N$ denotes the voltage and current samples, and $\sigma^2(\cdot)$ and $\sigma(\cdot,\cdot)$ are the variance and covariance operators, respectively. Being the time axis uniformly spaced, it is possible to write without loss of generality $t_k = (k-1)T_s$, where T_s is the sampling period. Thus, the above expressions reduce to

$$\left.\frac{dv}{dt}\right|_{\text{est}} = \frac{12}{T_s}\frac{\sum_k (k-1)v_k - \frac{N-1}{2}\sum_k v_k}{N(N^2-1)} \tag{6}$$

$$\left.\frac{di}{dt}\right|_{\text{est}} = \frac{12}{T_s}\frac{\sum_k (k-1)i_k - \frac{N-1}{2}\sum_k i_k}{N(N^2-1)}. \tag{7}$$

Other estimation algorithms could be employed, but they would lead to very similar results, because the uncertainty on the time axis is negligible and there are no significant outliers among the fitted samples.

As anticipated, the ohmic resistance can be calculated from the ratio between these two slopes

$$R_{\text{ohm,est}} = -\frac{\left.\frac{dv}{dt}\right|_{\text{est}}}{\left.\frac{di}{dt}\right|_{\text{est}}}. \tag{8}$$

Two estimates of R_{ohm} could be then obtained in each switching period, one during the increasing current ramp (T_{ON}) and another one during the decreasing current ramp (T_{OFF}). However, the very short switching period compared with the time scales on which the ohmic resistance is expected to vary suggests to calculate an average estimate of R_{ohm} on a longer time window (e.g., 0.1 s), to decrease the associated uncertainty. It should be noted that the number of samples used for the linear regression is generally different during T_{ON} and T_{OFF} (depending on the converter duty cycle), and it is also generally different in two consecutive increasing or decreasing ramps because of the time-varying switching frequency and the lack of synchronization between signal acquisition and converter switching. Thus, each ramp slope estimate is characterized by its own uncertainty, depending on the number of samples involved in the calculation, which must be taken into account in a weighted average algorithm to calculate the best estimate of R_{ohm} in the chosen time window.

The propagation of the voltage and current uncertainties through the linear regression algorithm used to identify the slope of the voltage and current ramps can be evaluated by standard propagation rules applied to (6) and (7), assuming constant uncertainties $u(v)$ and $u(i)$ for all voltage and current samples, respectively, arising from random uncertainty sources, thus without any correlation between different samples. These assumptions lead to the following expressions:

$$u\left(\left.\frac{dv}{dt}\right|_{\text{est}}\right) = \sqrt{\frac{12}{N(N^2-1)}}\frac{u(v)}{T_s} \tag{9}$$

$$u\left(\left.\frac{di}{dt}\right|_{\text{est}}\right) = \sqrt{\frac{12}{N(N^2-1)}}\frac{u(i)}{T_s}. \tag{10}$$

In the selected time window, the slopes of different ramps having the same sign are not expected to show significant variations, and thus a weighted average can be calculated as the slope best estimate, where the weighting coefficients are the inverse of the uncertainties (9) and (10) squared. The best estimate of the ohmic resistance evaluated during T_{ON} is therefore given by

$$\overline{R_{\text{ohm,est,ON}}} = -\frac{\sum_r N_{\text{ON},r}\left(N_{\text{ON},r}^2-1\right)\left.\frac{dv}{dt}\right|_{\text{est,ON},r}}{\sum_r N_{\text{ON},r}\left(N_{\text{ON},r}^2-1\right)\left.\frac{di}{dt}\right|_{\text{est,ON},r}} \tag{11}$$

and similarly for T_{OFF}

$$\overline{R_{\text{ohm,est,OFF}}} = -\frac{\sum_r N_{\text{OFF},r}\left(N_{\text{OFF},r}^2-1\right)\left.\frac{dv}{dt}\right|_{\text{est,OFF},r}}{\sum_r N_{\text{OFF},r}\left(N_{\text{OFF},r}^2-1\right)\left.\frac{di}{dt}\right|_{\text{est,OFF},r}} \tag{12}$$

where the index r denotes the different considered ramps.

Finally, a weighted average between the two ohmic resistance estimates obtained during T_{ON} and T_{OFF} should be evaluated, with the same approach followed above. An approximate expression can be derived by assuming that the average slopes of the ramps in T_{ON} and T_{OFF} (both voltage and current) are inversely proportional to the average number of samples in these ramps, being them inversely proportional to δ and $1-\delta$, respectively. From this assumption, the following proportionality can be derived:

$$u^2\left(\overline{R_{\text{ohm,est,ON}}}\right) \propto \frac{\left(\sum_r N_{\text{ON},r}\right)^2}{\sum_r N_{\text{ON},r}\left(N_{\text{ON},r}^2-1\right)} \tag{13}$$

$$u^2\left(\overline{R_{\text{ohm,est,OFF}}}\right) \propto \frac{\left(\sum_r N_{\text{OFF},r}\right)^2}{\sum_r N_{\text{OFF},r}\left(N_{\text{OFF},r}^2-1\right)} \tag{14}$$

and the inverse of these values can be used as weighting coefficients for the average between $\overline{R_{\text{ohm,est,ON}}}$ and $\overline{R_{\text{ohm,est,OFF}}}$.

The results thus obtained are expected to have an accuracy comparable with the results provided by the most accurate Fourier transform approach described in Section IV-A, but with a significantly lower computational burden suitable for real-time implementation, as confirmed by the experimental results reported in Section VI.

V. Experimental Setup

The proposed measurement technique was tested on a single PEM cell, although its applicability can be extended to FC stacks of several cells, more commonly employed in commercial applications, as discussed in the following.

A photograph of the experimental setup is shown in Fig. 6. The employed cell has an active area of 23 cm^2 and it is composed of commercial materials, in particular a Nafion 212 membrane as electrolyte (50-μm thickness) and a gas diffusion electrode reference sample (E-TEK LT140).

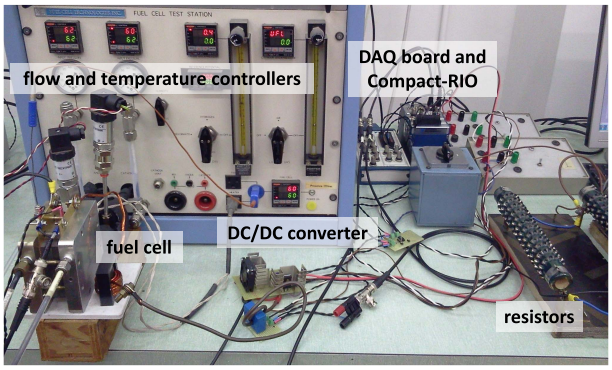

Fig. 6. Photograph of the experimental setup.

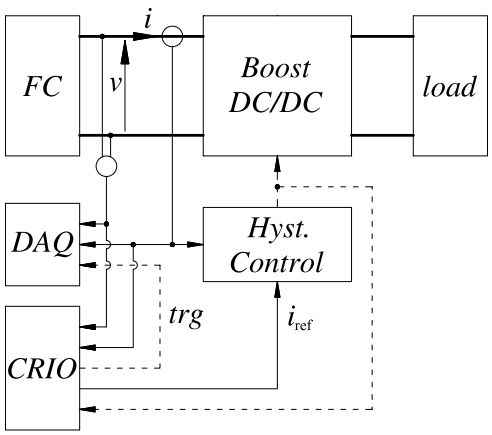

Fig. 7. Schematic of the connections among the employed devices.

The cell is fed with pure hydrogen and air at the anode and cathode, respectively, whose flow rates are measured and controlled by calibrated flow meters. Before entering the cell, both hydrogen and air are humidified through saturators, whose temperatures are controlled to achieve the desired relative humidity. Finally, the cell temperature is also controlled.

The cell is directly connected to a low-voltage dc/dc boost converter specifically designed for this application, whose output is in turn connected to a resistive load. The converter input inductance was designed to produce a current ripple with a peak-to-peak amplitude below 5% of the cell dc current at 10 A, when the converter switching frequency is 10 kHz. This amplitude limit is believed to be a reasonable value for the considered application, although it is difficult to find a generally accepted indication of the maximum allowed ripple because the evaluation of the associated negative effects on the FC performance (such as loss increase, possible damages and durability decrease) is not straightforward [22], [27]–[30].

The FC current (i.e., the converter input current) is measured by a closed-loop Hall-effect current transducer and it is controlled using a Schmitt trigger whose reference signal (either constant or slowly varying to introduce low-frequency perturbations) is generated by a reconfigurable input/output system (NI Compact-RIO 9014). The same system is used to acquire the cell voltage and current (with a 16-bit resolution and 10^5-samples/s sampling frequency), together with the digital switching signal (with a time resolution of 0.4 μs), while providing real-time processing of the signals according to the time-domain approach described in Section IV-B. The cell voltage and current are also acquired by a 16-bit data acquisition (DAQ) system (NI 6251) synchronized with the Compact-RIO, with a higher sampling frequency ($5 \cdot 10^5$ samples/s), for a more accurate offline elaboration aiming at comparing different identification algorithms for the ohmic resistance. A schematic of the connections among all the employed devices is shown in Fig. 7.

A first real-time data processing is performed in the Xilinx Virtex-II 3-million-gate FPGA included in the Compact-RIO. The start instant of each voltage and current ramp is identified based on the digital switching signal, and the slope of each ramp is estimated according to the linear regression expressions in (6) and (7). The execution of this algorithm is synchronized with the voltage and current acquisition, so that the sums in (6) and (7) are updated after the acquisition of each new sample. To avoid the effects of numerical errors that may arise due to the 16-bit numerical format employed in the FPGA, the average values of the voltage and current ramps are subtracted from the next acquired ramps, so that in steady-state conditions, the dc components of the processed signals are much smaller than the peak-to-peak amplitudes. The estimated increasing and decreasing ramp slope values in each switching period, together with the number of samples on which the estimation was based, are then passed to a 400-MHz-clock real-time processor that is also included in the Compact-RIO, where the weighted averages (11) and (12) are calculated and the best estimate of the ohmic resistance in the selected time window (1000 switching periods) is finally evaluated.

It is worth noting that an accurate ohmic resistance estimate can be obtained in a quite short time window (about 0.1 s in this case) compared with the time scales in which the cell ohmic resistance is expected to change due to water content variations (tens of seconds or minutes). Thus, in case of FC stacks, which are typically employed in commercial applications, a multiplexed architecture can be easily employed to monitor the ohmic resistance of each cell (or small groups of cells) in the stack, without increasing the cost and complexity of the required instrumentation.

VI. Experimental Results

First experimental tests were performed in stationary conditions, with the cell running at a medium-level dc current of 9.2 A, corresponding to 0.4 A/cm^2. The cell temperature was kept constant at 60 °C and the gas flow rates were set to 0.2 and 1.0 Nl/min for hydrogen and air, respectively, with 90% relative humidity for both gases. Finally, the resistive load was adjusted to make the converter work with a duty cycle around 0.7. The current and voltage waveforms measured by the DAQ system in these conditions are reported in Fig. 8. It can be seen that the switching frequency is not constant and its average value is slightly smaller than the expected value according to the design specifications (10 kHz).

The ohmic resistance values estimated offline from these signals according to the time-domain approach described in Section IV-B are reported in Fig. 9 (line R1), in a time

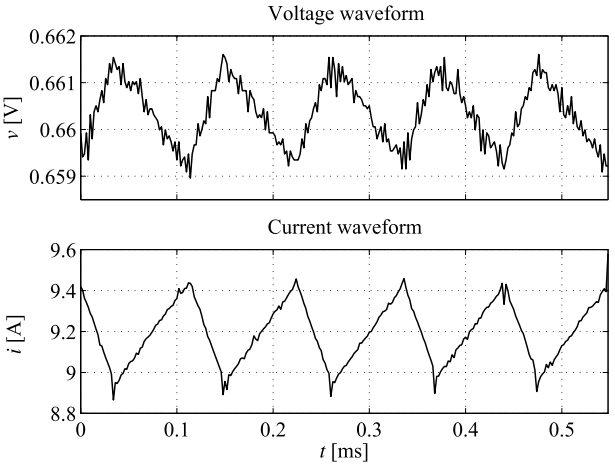

Fig. 8. Current and voltage waveforms measured by the DAQ system.

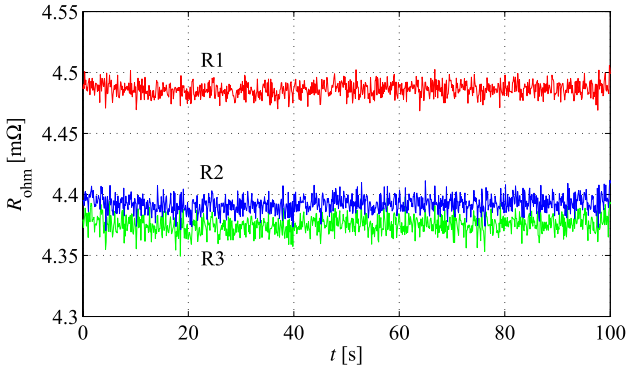

Fig. 9. Ohmic resistance values estimated offline by different identification methods, namely, the proposed time-domain analysis with (red line R1) and without (green line R3) elimination of extreme ramp values and frequency-domain analysis (blue line R2).

interval of 100 s. Each value is measured in a time window of 1000 switching periods, corresponding to about 0.1 s, by neglecting the two extreme voltage and current samples at the beginning and at the end of each ramp to prevent possible commutation disturbances from affecting the slope estimates. The results thus obtained are compared with those provided by the frequency-domain analysis, also reported in Fig. 9 (line R2). In this case, each resistance value was obtained by applying the Fourier transform on a fixed time window of 0.1 s and averaging the resistance values calculated from the 100 harmonic components around the most significant one, weighted by the square of their amplitudes, according to what was discussed in Section IV-A.

The standard deviation of the R_{ohm} estimates is a key parameter for this diagnostic technique, because it defines the minimum variation of the ohmic resistance that can be distinguished from noise. It is worth noting that the two above-mentioned estimates of R_{ohm} have similar standard deviations (lower than 0.01 mΩ in both cases), but there is a significant difference between their mean values. Such a difference can be attributed to the disturbances introduced by commutations, which in practice affect only the results obtained by the Fourier transform. To confirm this hypothesis, the ohmic resistance values estimated from the time-domain analysis

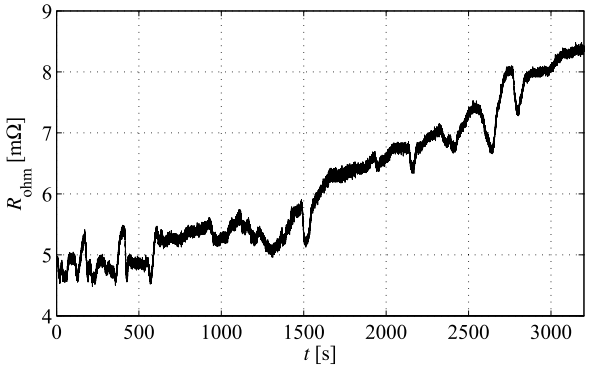

Fig. 10. Real-time ohmic resistance estimate calculated by the Compact-RIO during a membrane dehydration transient induced by decreasing the inlet gas relative humidity.

without discarding any voltage or current sample are also reported in Fig. 9 (line R3), and they are in good agreement with the results provided by the frequency-domain analysis. Therefore, it seems reasonable to conclude that the R_{ohm} estimate in R1 should be regarded as the most accurate one. As a further confirmation, it can be also mentioned that in this case, there is compatibility between the R_{ohm} estimates obtained during T_{ON} and T_{OFF}, while this is not the case for the values in R3.

Finally, the results obtained from the real-time identification algorithm implemented in the Compact-RIO are reported in Fig. 10. To verify whether the measurement accuracy is good enough to allow an effective and fast detection of ohmic resistance variations arising from faults or nonproper FC operation, a membrane dehydration transient was induced during the test by gradually decreasing the inlet gas relative humidity from 90% to 50%. As expected, the standard deviation of the R_{ohm} values is now higher than that for the DAQ measurements (about 0.04 mΩ) because of the lower sampling frequency and the worse converter resolution, but it is still small enough to allow detecting the ohmic resistance increase due to dehydration, as well as the small oscillations that characterize the FC operation with low membrane humidification [31].

VII. Conclusion

A low-cost diagnostic method for PEM FCs was presented, based on the use of the ripple produced by switch-mode power converters for the identification of relevant indicators of the FC state of health, suitable for commercial applications. In more details, this paper dealt with the measurement processing issues that arise when the ripple is produced by a dc/dc converter with hysteresis control, causing the ripple waveform to have a variable frequency.

While an accurate processing of the FC response to this high-frequency ripple is important to estimate the equivalent ohmic resistance of the cell, suitable for membrane dehydration diagnosis, conventional frequency-domain techniques are not able to provide accurate results or they require a computational burden not suitable for real-time implementation in low-cost commercial applications. On the contrary, a time-domain approach based on a general circuital

model of the FC was shown to provide accurate results with a simple algorithm suitable for real-time implementation.

The proposed method was tested on a single PEM FC, although it can be conceptually extended to stacks composed of several cells, and it was compared with a classic frequency-domain analysis. The identification algorithm was then implemented in an FPGA and a real-time processor to test its application to online diagnosis, with low sampling frequency to validate the proposed approach even when less accurate measurements (provided by low-cost instrumentation) are available.

Ongoing research is aiming at addressing the additional issues that arise when applying the proposed technique to FC stacks of several cells and at including the analysis of the cell response to low-frequency perturbations in the real-time elaboration algorithm, for a more complete state-of-health diagnosis.

REFERENCES

[1] F. Barbir, *PEM Fuel Cells: Theory and Practice*, 2nd ed. Amsterdam, The Netherlands: Elsevier, 2013.

[2] Y. Wang, K. S. Chen, J. Mishler, S. C. Cho, and X. C. Adroher, "A review of polymer electrolyte membrane fuel cells: Technology, applications, and needs on fundamental research," *Appl. Energy*, vol. 88, no. 4, pp. 981–1007, 2011.

[3] W. Dai *et al.*, "A review on water balance in the membrane electrode assembly of proton exchange membrane fuel cells," *Int. J. Hydrogen Energy*, vol. 34, no. 23, pp. 9461–9478, 2009.

[4] N. Yousfi-Steiner, P. Moçotéguy, D. Candusso, D. Hissel, A. Hernandez, and A. Aslanides, "A review on PEM voltage degradation associated with water management: Impacts, influent factors and characterization," *J. Power Sour.*, vol. 183, no. 1, pp. 260–274, 2008.

[5] X. Yuan, H. Wang, J. C. Sun, and J. Zhang, "AC impedance technique in PEM fuel cell diagnosis—A review," *Int. J. Hydrogen Energy*, vol. 32, no. 17, pp. 4365–4380, 2007.

[6] J. M. Le Canut, R. M. Abouatallah, and D. A. Harrington, "Detection of membrane drying, fuel cell flooding, and anode catalyst poisoning on PEMFC stacks by electrochemical impedance spectroscopy," *J. Electrochem. Soc.*, vol. 153, no. 5, pp. A857–A864, 2006.

[7] W. Mérida, D. A. Harrington, J. M. Le Canut, and G. McLean, "Characterisation of proton exchange membrane fuel cell (PEMFC) failures via electrochemical impedance spectroscopy," *J. Power Sour.*, vol. 161, no. 1, pp. 264–274, 2006.

[8] N. Fouquet, C. Doulet, C. Nouillant, G. Dauphin-Tanguy, and B. Ould-Bouamama, "Model based PEM fuel cell state-of-health monitoring via ac impedance measurements," *J. Power Sour.*, vol. 159, no. 2, pp. 905–913, 2006.

[9] T. Kurz, A. Hakenjos, J. Krämer, M. Zedda, and C. Agert, "An impedance-based predictive control strategy for the state-of-health of PEM fuel cell stacks," *J. Power Sour.*, vol. 180, no. 2, pp. 742–747, 2008.

[10] M. F. Mathias and S. A. Grot, "System and method for controlling the humidity level of a fuel cell," U.S. Patent 6 376 111, Apr. 23, 2002.

[11] M. Hinaje, I. Sadli, J.-P. Martin, P. Thounthong, S. Raël, and B. Davat, "Online humidification diagnosis of a PEMFC using a static DC–DC converter," *Int. J. Hydrogen Energy*, vol. 34, no. 6, pp. 2718–2723, 2009.

[12] G. Dotelli, R. Ferrero, P. G. Stampino, S. Latorrata, and S. Toscani, "Diagnosis of PEM fuel cell drying and flooding based on power converter ripple," *IEEE Trans. Instrum. Meas.*, vol. 63, no. 10, pp. 2341–2348, Oct. 2014.

[13] G. Dotelli, R. Ferrero, P. G. Stampino, S. Latorrata, and S. Toscani, "Testing of a diagnostic technique for a single PEM fuel cell based on a DC/DC converter," in *Proc. IEEE Int. Workshop AMPS*, Aachen, Germany, Sep. 2014, pp. 1–5.

[14] G. Dotelli, R. Ferrero, P. G. Stampino, S. Latorrata, and S. Toscani, "PEM fuel cell drying and flooding diagnosis with signals injected by a power converter," *IEEE Trans. Instrum. Meas.*, to be published, doi: 10.1109/TIM.2015.2406051.

[15] N. Katayama and S. Kogoshi, "Real-time electrochemical impedance diagnosis for fuel cells using a DC–DC converter," *IEEE Trans. Energy Convers.*, vol. 30, no. 2, pp. 707–713, Jun. 2015.

[16] Y. H. Li, S. Rajakaruna, and S. S. Choi, "Control of a solid oxide fuel cell power plant in a grid-connected system," *IEEE Trans. Energy Convers.*, vol. 22, no. 2, pp. 405–413, Jun. 2007.

[17] K. Green and J. C. Wilson, "Future power sources for mobile communications," *Electron. Commun. Eng. J.*, vol. 13, no. 1, pp. 43–47, 2001.

[18] A. T-Raissi and D. L. Block, "Hydrogen: Automotive fuel of the future," *IEEE Power Energy Mag.*, vol. 2, no. 6, pp. 40–45, Nov./Dec. 2004.

[19] M. Mohr, W. T. Franke, B. Wittig, and F. W. Fuchs, "Converter systems for fuel cells in the medium power range—A comparative study," *IEEE Trans. Ind. Electron.*, vol. 57, no. 6, pp. 2024–2032, Jun. 2010.

[20] P. Thounthong, S. Raël, and B. Davat, "Control algorithm of fuel cell and batteries for distributed generation system," *IEEE Trans. Energy Convers.*, vol. 23, no. 1, pp. 148–155, Mar. 2008.

[21] P. Thounthong, S. Raël, and B. Davat, "Analysis of supercapacitor as second source based on fuel cell power generation," *IEEE Trans. Energy Convers.*, vol. 24, no. 1, pp. 247–255, Mar. 2009.

[22] R. Ferrero, M. Marracci, M. Prioli, and B. Tellini, "Simplified model for evaluating ripple effects on commercial PEM fuel cell," *Int. J. Hydrogen Energy*, vol. 37, no. 18, pp. 13462–13469, 2012.

[23] C. Wang, M. H. Nehrir, and S. R. Shaw, "Dynamic models and model validation for PEM fuel cells using electrical circuits," *IEEE Trans. Energy Convers.*, vol. 20, no. 2, pp. 442–451, Jun. 2005.

[24] N. Wagner, "Characterization of membrane electrode assemblies in polymer electrolyte fuel cells using a.c. impedance spectroscopy," *J. Appl. Electrochem.*, vol. 32, no. 8, pp. 859–863, 2002.

[25] K. R. Cooper and M. Smith, "Electrical test methods for on-line fuel cell ohmic resistance measurement," *J. Power Sour.*, vol. 160, no. 2, pp. 1088–1095, 2006.

[26] R. Pintelon and J. Schoukens, *System Identification: A Frequency Domain Approach*, 2nd ed. Hoboken, NJ, USA: Wiley, 2012.

[27] R. S. Gemmen, "Analysis for the effect of inverter ripple current on fuel cell operating condition," *J. Fluids Eng.*, vol. 125, no. 3, pp. 576–585, 2003.

[28] W. Choi, J. W. Howze, and P. Enjeti, "Development of an equivalent circuit model of a fuel cell to evaluate the effects of inverter ripple current," *J. Power Sour.*, vol. 158, no. 2, pp. 1324–1332, 2006.

[29] B. Wahdame *et al.*, "Impact of power converter current ripple on the durability of a fuel cell stack," in *Proc. IEEE ISIE*, Cambridge, U.K., Jun./Jul. 2008, pp. 1495–1500.

[30] R. Ferrero, M. Marracci, and B. Tellini, "Single PEM fuel cell analysis for the evaluation of current ripple effects," *IEEE Trans. Instrum. Meas.*, vol. 62, no. 5, pp. 1058–1064, May 2013.

[31] G. Dotelli, R. Ferrero, P. G. Stampino, and S. Latorrata, "Analysis and compensation of PEM fuel cell instabilities in low-frequency EIS measurements," *IEEE Trans. Instrum. Meas.*, vol. 63, no. 7, pp. 1693–1700, Jul. 2014.